J Solid State Electrochem (2012) 16:213–218
DOI 10.1007/s10008-011-1307-x

ORIGINAL PAPER

Physical and photoelectrochemical characterization of $CuCrO_2$ single crystal

Wahiba Ketir · Souad Saadi · Mohamed Trari

Received: 11 November 2010 / Accepted: 7 January 2011 / Published online: 3 February 2011

Abstract $CuCrO_2$ single crystal, elaborated by the flux method, is a narrow-band-gap semiconductor crystallizing in the delafossite structure with an indirect optical transition at 2.12 eV. The relatively longer Cu–Cu is consistent with the semi-conducting behavior. The conductivity in the (001) plans is thermally activated and occurs predominantly by small polaron hopping through mixed-valence states $Cu^{+/2+}$ in conformity with a classical dielectric behavior. The activation energy (0.05 eV) gave an effective mass of $9m_o$, indicating that the levels in the vicinity of the Fermi level E_f are strongly localized. The oxide shows an excellent chemical stability over the whole pH range; the semi-logarithmic plot gave an exchange current density of 0.7 mA cm^{-2} and a corrosion potential of 0.18 $V_{/SCE}$ in KOH (0.5 M) electrolyte. The electrochemical study is confined in (001) plans, and reversible oxygen intercalation is evidenced from the cyclic voltammetry. The Mott–Schottky plot (C^{-2}-V) is characteristic of *p* type conduction and exhibits a linear plot from which a flat band potential of +0.21 $V_{/SCE}$ and a holes density N_A of 5.06×10^{14} cm^{-3} were obtained. The photocurrent is due to Cu^+: $d\rightarrow d$ transition and the valence band is positioned at 5.34 eV below vacuum.

W. Ketir
Technical and Scientific Research Centre of Physico-Chemical Analysis (CRAPC),
BP 248,
RP 16004, Algiers, Algeria

W. Ketir · S. Saadi · M. Trari (✉)
Laboratory of Storage and Valorization of Renewable Energies,
Faculty of Chemistry (USTHB),
BP 32,
16111, Algiers, Algeria
e-mail: solarchemistry@gmail.com

Keywords $CuCrO_2$ · Single crystal · Delafossite · Dielectric · Photoelectrochemical

Introduction

The search of novel materials for the photoelectrochemical (PEC) devices has gained increasing interest in the solar energy conversion [1–3]. The delafossites $Cu^+M^{3+}O_2$ where M is commonly a first-row transition metal have drawn considerable attention because of their potential applications in many areas like thermoelectricity [4], optoelectronic devices [5], energetic fuels [6], and more recently, environmental protection [7]. The structure of $CuMO_2$ is highly anisotropic with infinite $[MO_2]$ layers extending in the basal plans and presents an interest both from the basic and applied point of view. The small gap (*E*g) and the chemical stability make them attractive for PEC applications. Both the valence and conduction band are made up of Cu-*3d* orbital, which are pH-insensitive [8], and this property has yet been exploited for the water splitting [9]. However, whereas the semi conducting properties of single crystal has given rise to some studies and interpretations, the PEC characterization has not been reported before now. The oxide is expected to be insulating, but the transport properties can be slightly tailored by oxygen insertion in the Cu-plans, giving the opportunity for characterizing the oxide photoelectrochemically [10]. In addition, the effect of anisotropy of delafossite in the electrochemical behavior is not well understood yet, and the intrinsic properties can be obtained only on single crystal.

In a previous paper, we reported the physical properties of $CuAlO_2$ [11]. In extension, the present paper deals with $CuCrO_2$ single crystals elaborated by the flux method under oxygen-free atmosphere, the physical properties and PEC

characterization. $CuCrO_2$ is the most stable oxide among the congeners investigated nowadays. A slight deviation from the stoichiometry improves the electrical conductivity [12] and permits the PEC characterization.

Experimental

The growth of single crystals has been performed in a platinum crucible standing in a vertical programming furnace under argon flow to prevent oxidation of Cr(III). A mixture of extra pure CuO (10 g Merck, dried at 400 °C) and Cr_2O_3 (30 g Fluka, prefired at 600 °C) was heated at 1,160 °C (60 °C/h) and maintained 12 h at that temperature. The cooling rate (1.5 °C h^{-1}) was controlled from 1,140 to 700 °C below which the sample was cooled to room temperature by turning off the furnace. The chemical composition of crystals was confirmed by electronic microprobe analysis. The electrical contact on (001) oriented single crystal was made with silver cement. Dielectric measurements as a function of temperature were performed using Agilent 4263 B LCR Meter. The temperature dependence of the thermopower ($S = \Delta V/\Delta T$) was determined in a home-made equipment, the induced emf ΔV was measured by a differential electrometer (Tacussel ARIES 2000) with an input impedance of 10^{12} Ω. The precision was dependant on the quality of thermal contact, and the crystal was held between sinks to ensure good electrical and thermal contact. The small heat conductivity made it possible to use a large temperature gradient and to continue the measurement down to liquid nitrogen temperature.

For PEC study, the crystal was encapsulated in Teflon insulation with epoxy resin. The intensity-potential J(V) characteristics and impedance measurements were performed in a double-walled electrochemical cell, connected to a thermostated bath whose temperature was regulated at 25 °C. Pt electrode (Tacussel) served as auxiliary electrode and the potential of the working electrode (WE) was controlled by a Voltalab PGZ301 potentiostat (Radiometer). A saturated calomel electrode (SCE) connected to the solution via a salt bridge was used as reference electrode. The KOH (0.5 M) solution, used for its high electroconductivity, was continually flushed by nitrogen. Unless stated otherwise, the potential scan was 10 mV s^{-1}. The capacitance was determined as a function of the potential with a rate of 10 mV $step^{-1}$. To facilitate the light transmission, WE was positioned midway between the anode and the cell. WE was irradiated through a flat optical window by a 650 W halogen lamp (Dyr. General Electric), whose output was passed through a series of filters (PHYWE). The flux intensity was measured with a calibrated light meter (Testo 545). The solutions have been prepared from reagents of analytical grade quality and distilled water.

Results and discussion

Single crystals with platelet morphology are black in appearance with a typical size of $0.2\times0.3\times0.02$ mm^3. $CuCrO_2$ crystallizes in a rhombohedral symmetry with the space group $R\bar{3}m(D^5_{3d})$. The lattice constants in the hexagonal description: a_h=0.297(4) and c_h=1.710(1)nm, agree with those of the literature data [13]. The structure can be visualized as close-packed layers of Cr^{3+} sharing common edges octahedra (Fig. 1). The layers are linked to each other by linear CuO_2^{3-} 'dumb-bell' unit parallel to c-axis. Three (CrO_6) layers are sandwiched between Cu monolayer giving $CuCrO_2$ anisotropic properties. Crystallographic data, selected inter-atomic distances, and bond angles of $CuCrO_2$ are given in Table 1. The bond lengths Cu-O (0.1881 nm) and Cr-O (0.1972 nm) are in perfect agreement with those calculated from the Shannon ionic radii, respectively (0.1850 nm) and (0.1987 nm): $^{II}Cu^{+} = 0.046$, $^{VI}Cr^{3+} = 0.0615$ and $^{II}O^{2-} = 0.138$nm, II, VI, and IV are the coordination numbers. The closeness of the Cu-O lengths confirms the ionicity of the chemical bond.

Cu^+ has d^{10} closed-shell configuration and the distance Cu^+–Cu^+, equal to a-parameter, is larger than the inter-ionic cation of $3d$ overlap below, which itinerant electrons ensues (0.1565 nm)[1] and the oxide is expected to be insulating. However, the electrical properties of $CuCrO_2$ are slightly enhanced by oxygen intercalation. Indeed, the 2D structure offers a pathway with reduced activation energy for oxygen diffusion. The holes concentration is based on a charge balance on the assumption that each inserted O^{2-} yields two holes to the valence band. The conductivity is highly anisotropic, being much greater perpendicular to the c-axis with a conductivity $\sigma_\perp$ of 3.36×10^{-5} Ω^{-1} cm^{-1}. $\sigma_\perp$ increases with increasing temperature (Fig. 2) and obeys to an exponential law ($\sigma T = \sigma_o e^{-E\sigma\perp/RT}$) indicating semiconducting like behavior. At high temperatures, the evolution is not monotonic and the slope $d\ log\sigma/d\ (1/T)$ decreases with decreasing temperature. An activation energy $E_{\sigma\perp}$ of 50 meV was calculated in the temperature range (300–350 K). The relaxation time for dipole movement is high, and the dielectric constant (ε) is attributed to the large dimension of single crystal; it is low and is due to the electronic polarizability and to the existence of a space charge region (Fig. 3).

[1] Calculated from the lattice constant (0.3615 nm) of copper crystallizing in a face-centered cubic.

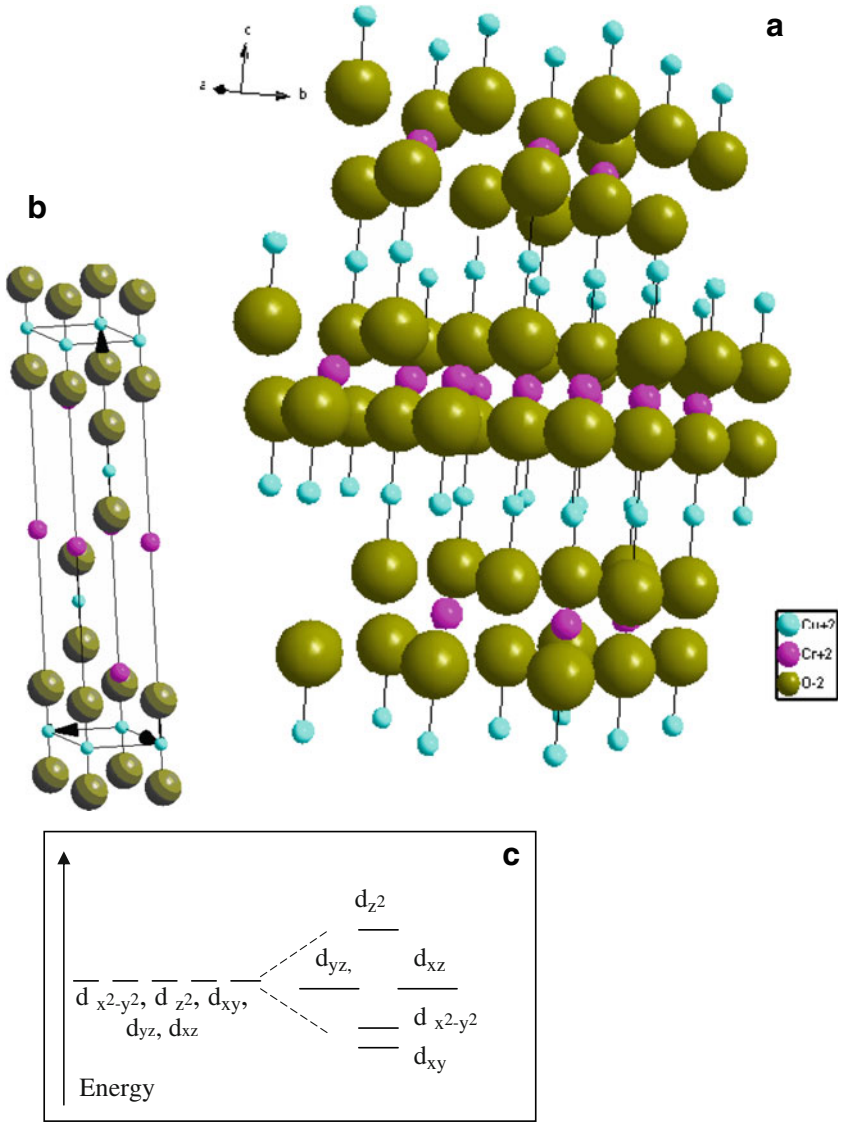

Fig. 1 **a** Crystal structure of the delafossite $CuCrO_2$; **b** Unit cell of one polymorph of the delafossite structure, the layers of Cu^+ and CrO_2 are stacked alternatively along the [001] direction; **c** Energies of the Cu-*3d* orbitals in a linear field CuO_2^{3-}

Table 1 Structural data relative to $CuCrO_2$ single crystal

Cristal data	Space group		$R\bar{3}m$
	Unit cell dimensions		a = 2.9747(14) Å
			c = 17.1015(5) Å
	Cell volume		131.05(9) Å^3
	Z		3
Atomic coordinates		x y z	
	Cu	0 0 0	
	Cr	0 0 1/2	
	O	0 0 0.108(2)	
Interatomic distances (nm)	Cu-O	0.1847	(×2)
	Cr-O	0.1989	(×6)
Angles	O—Cu—O		180°
	Cu—O—Cr		120.29°
	Cr^i—O—Cr^{ii}		96.80°
Symmetry codes	(i) 1/3 + x , 2/3 + y , -1/3 + z; (ii) 1/3 + x , -1/3 + y , -1/3 + z.		

With the coordinates of equivalent positions and symmetry code (Wyckoff notation)

The low conductivity indicates that the Cu: *3d* electrons are strongly localized as evidenced by the large thermopower (Fig. 4). The conduction occurs predominantly by low polaron hopping between mixed-valences $Cu^{+/2+}$ based on a strong lattice distortion [14], and in such a case, the thermopower is given by [15]:

$$S = \left(\frac{k}{e}\right)\frac{\Delta E_{\perp}}{kT} + A = \left(\frac{k}{e}\right)\ln\left(\frac{N_O}{N_A}\right) \quad (1)$$

where A is dimensionless constant, which depends on the scattering mechanism. N_o is the density of available sites, assimilated to the Cu^+ concentration (2.08×10^{22} cm^{-3}) and calculated from the experimental density of poly crystal (5.35 g cm^{-3}) and N_A is the density of polarons taking part in the conduction process. At 250 K, the S value (2,070 μV K^{-1}) gives an activation energy $E_{S\perp}$ basal plane of 517 meV and a ratio N_A/N_o of 2.43×10^{-8}. The large difference in the energies between $E_{\sigma\perp}$ and $E_{S\perp}$ is the hallmark of mechanism by small polaron hopping conduction where nearly all Cu^{2+} acceptors are localized at room temperature, i.e., most holes are trapped in surface-state polarons. The holes move in the narrow Cu-*3d* band, not exceeding 2 eV leading to a low mobility μ_h (0.41 cm^2 V^{-1} s^{-1}), calculated from the relation ($\sigma = e\ \mu_h\ N_A$). Cu^{2+} has been observed by electron paramagnetic resonance in polycrystal and may contribute to lower the mobility. The mobility in single crystal is higher than in ceramic, since it is not limited by the grain boundaries. The synthesis was performed under argon atmosphere, and the doping level is relatively small. Therefore, $E_{\perp}$ value suggests that the Fermi level shifts away from the valence band, and this means that the crystal approaches intrinsic-type conductivity with no shallow levels. Based on the Ioffe–Regel criteria, Mott outlined that for insulating materials, the disorder is large enough that the quantity (k_f l) becomes less than unity, k_f being the wave vector and l the mean-free path. The small polaron has low mobility and behaves like heavy particle with a finite mean-free path (l). The enhanced effective mass $m^*(\sim 9m_o)$ [2] is due to the fact that the impurity band, originating from oxygen insertion, does not merge with the valence band and indicates a high density of states at the Fermi level E_f, m_o being the electron rest mass.

The oxide is chemically stable and does not dissolve even in strong mineral acids like $HClO_4$. The (001) plan has been used as active surface and the electrokinetic parameters deduced from the semi-log plot (Fig. 5 inset) gave an exchange current density of 0.7 mA cm^{-2} and a corrosion potential of 0.18 V_{ECS}. Much less is known about the oxygen intercalation in delafossites. A typical cyclic J (V) curve (Fig. 5) shows a rectifying junction at the

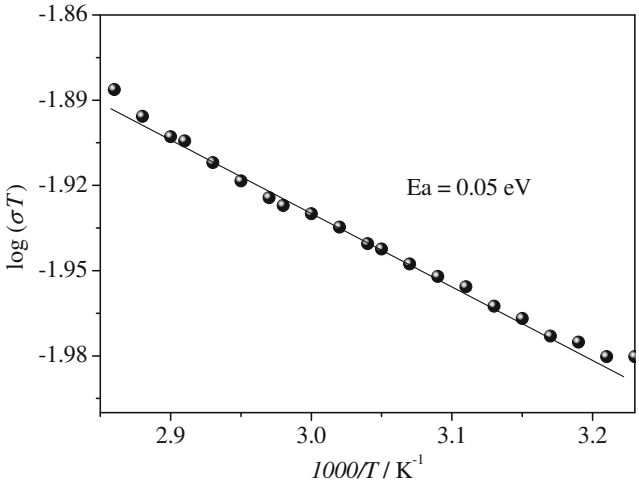

Fig. 2 A close view of log (σT) vs 1,000/T plot of $CuCrO_2$

electrolyte contact. The barrier nature is considered to be of Schottky-type (chemical diode) with a dark current J_d less than 0.1 mA cm^{-2}. Oxygen over stoichiometry is rather common, depending on the nature of the M cation, and $CuMO_{2+x}$ belong to class I in the Day and Robin classification, i.e., mixed valences in non-equivalent crystallographic sites. x can reach values as high as 0.6, involving consequently order–disorder phenomena [16]. Electrons are coming out from the copper planes, and the electrochemical reaction can be written:

$$CuCrO_2 + 2\tau OH^- \rightarrow CuCrO_{2+\tau} + \tau H_2O + 2\tau e^- \quad (2)$$

where τ stands for the amount of intercalated oxygen. The presence of two peaks indicates that $Cu^{+/2+}$ comes from two kinds of non-equivalent crystallographic sites. The existence of Cu^{3+} is doubtful in $CuCrO_2$ and one can anticipate that Cu^{2+} originating from oxygen insertion becomes less

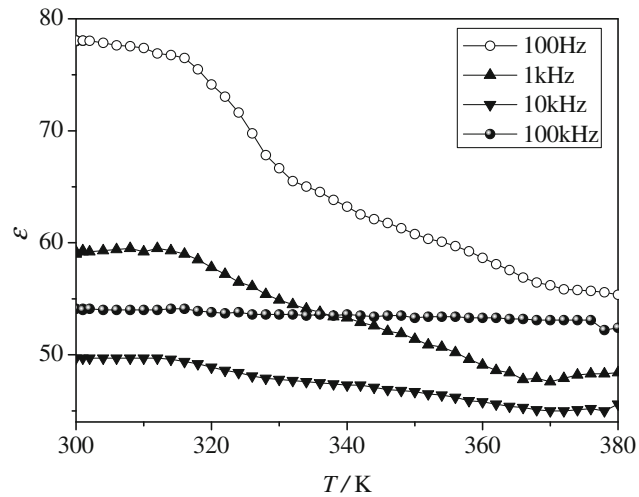

Fig. 3 The thermal variation of the dielectric constant at various frequencies

[2] Determined from the relation $E_\sigma = e^4 m^*/2(4\pi\varepsilon\varepsilon_o\hbar)^2$, ε_o being the dielectric constant of free space.

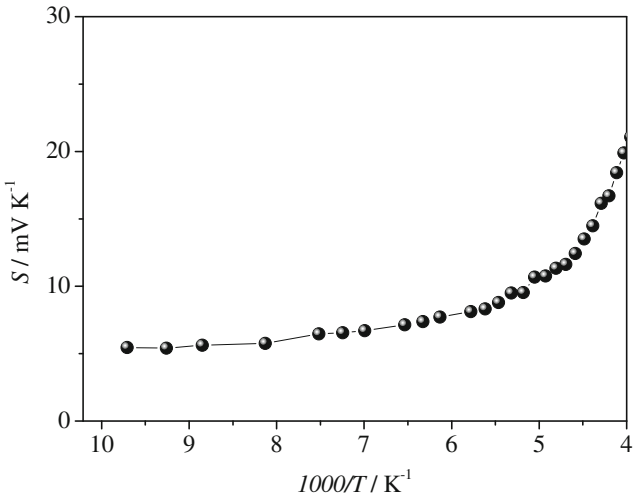

Fig. 4 Thermal dependence of the thermopower of $CuCrO_2$

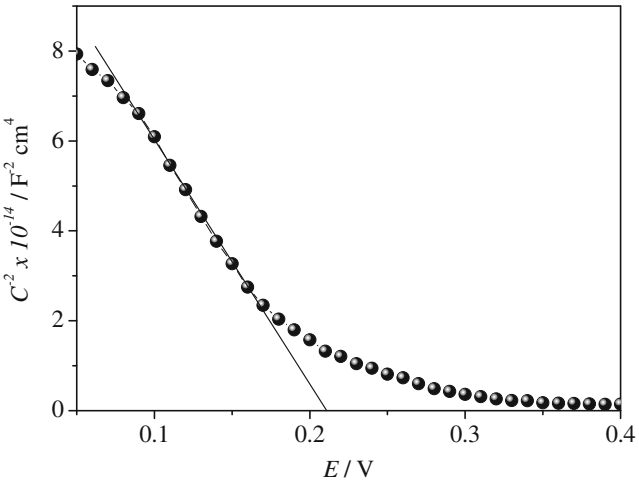

Fig. 6 The Mott–Schottky plot of $CuCrO_2$ in KOH (0.5 M) electrolyte

coordinate and easy to oxidize (peak −0.41 V, O_1) because of the lower potential barrier for the electron hopping than that coming from inside the lattice (peak −0.14 V, O_2). The charge under the peak O1, measured by area integration (~1.73 mC cm^{-2}) corresponds to the oxidation of ~10^{16} at Cu^+ cm^{-2}. The electrochemical peaks corroborate the weak delocalization of the Cu: *3d* electrons in conformity with the semi-conducting character of the single crystal. On the reverse scan, the two peaks located at −0.41 V (R_2) and −0.75 V (R_1) correspond respectively to the reversible reductions (O_2 and O_1) followed by oxygen desintercalation and below −1.2 V, the current shoots up drastically owing to the hydrogen evolution.

The increase of the photocurrent (J_{ph}), along the cathodic polarization lends a further support of *p* type conductivity. At sufficient negative potentials, J_{ph} reaches a limiting value, the magnitude of which was found to depend only on the flux intensity. Below −0.9 V, J_{ph} is superimposed to hydrogen evolution. The total capacitance is given by:

$$C^{-1} = (C_H)^{-1} + (C_{SC})^{-1} \tag{3}$$

where C_H and C_{SC} are respectively the capacitances of Helmoltz and space of charge region. Due to the low dielectric constant, one has $C_H >> C_{SC}$ and the term $1/C_H$ can be neglected. Hence, the capacitance at the interface is given by the Mott–Scottcky relation:

$$\frac{1}{{C_{SC}}^2} = \pm \frac{2}{e\varepsilon\varepsilon_0 N_A}\left(V - V_{fb} - \frac{kT}{e}\right) \tag{4}$$

The symbols are assigned to their usual significations. The negative slope confirms the *p* type character (Fig. 6) of

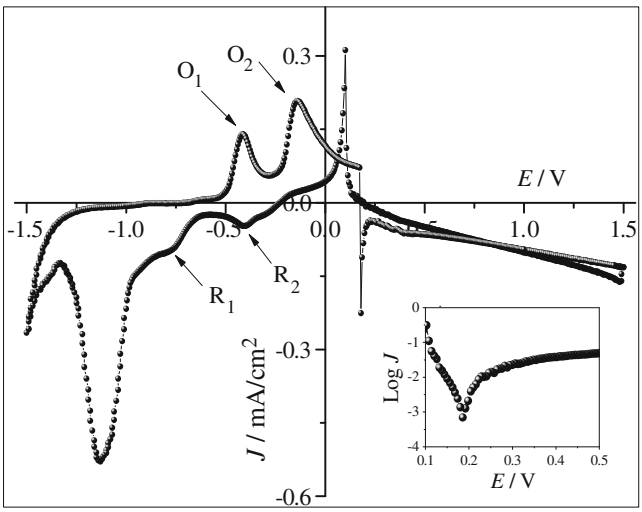

Fig. 5 Cyclic voltammetry of $CuCrO_2$ in KOH (0.5 M). Scan rate 10 mV/s. *Inset*: Semi-logarithmic plot log(*J*)-V

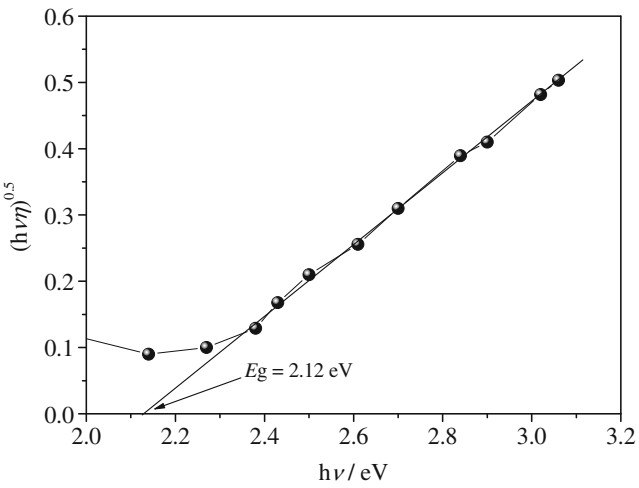

Fig. 7 The quantum efficiency of $(h\nu\eta)^{0.5}$ vs. the incident photon ($h\nu$)

$CuCrO_2$ crystal. The linear behavior (C^{-2}-V) indicates a constant holes density N_A (5.06×10^{14} cm^{-3}), whereas the flat-band potential V_{fb} (0.21 V) was deduced from the intersection of C^{-2} with the potential axis. The curvature for potential greater than ~0.25 V implies a predominance of the recombination process when one approaches the potential V_{fb} from below, while for potentials anodic of ~0.3 V, the recombination process of (electron/hole) pairs takes place preferentially. The position of the valence band is given by:

$$4.75 + eV_{fb} + 0.056\left(pH - pH_{pzc}\right) + E_{\perp} \quad (5)$$

pH_{pzc} is the pH at the point of zero charge ($pH–pH_{pzc}=5.9$) and 4.75 was the free energy of the electron vs. SCE. The valence band edge was therefore: 5.3±0.05 eV below the vacuum level and is made up mainly of Cu-*3d* orbitals. The electronic bands are predominantly Cu-*3d* orbital with a separation characterized by strength of the ligand field. Cu^+ is linearly coordinated and the band diagram is determined by CuO_2^{3-} unit, where only the transition $(Cu^+ \rightarrow Cu^+)$ can be involved in the energy range considered. It is of interest to describe briefly the origin of this trend in terms of the band structure. The degeneracy lift is determined by the linear field that splits the five Cu-*3d* orbital into a set of lower energy d_{xy} level, followed by $d_{x^2-y^2}$ and a set of doubly degenerate d_{xz} and d_{yz} separated from the higher d_{z^2} manifold by 1 eV (see Fig. 1. inset).

The strong hybridization raises the antibonding σ^* energy

The electrode was polarized at −0.44 V, and the quantum yield (η) was evaluated by dividing the electron flow in the external circuit (photocurrent subtracted from the dark current) by the incident photons flux (Φ_o) determined at each wavelength:The spectral photo-response has been measured in the range 400–1,000 nm and η is given by:

$$(\eta h\nu)^{2/m} = A(h\nu - Eg) \quad (6)$$

m is equal to 1 or 4, respectively, for direct and indirect transitions. The plot of $(\eta h\nu)^m$ against the incident energy $h\nu$ allows the determination of both the nature and the value of the transition. The indirect optical gap Eg (2.12 eV) is determined from the cross point of the extended plot of $(\eta h\nu)^{1/2}$ with the $h\nu$-axis (Fig. 7). The higher energy given in the literature [17] corresponds to the charge transfer O^{2-}: *2p* (oxygen)→*3d* (Cu^{2+}).

Conclusion

The physical and photoelectrochemical properties of $CuCrO_2$ single crystal elaborated by the flux method have been investigated for the first time. The structure is anisotropic and the study was confined on the (001) crystallographic planes. The order of magnitude of the conductivity and thermopower showed semi-conducting like properties, and the conduction occurs by small hopping polaron. The reversibility of oxygen insertion was proven by electrochemical peaks in the intensity-potential characteristics. The cathodic photocurrent confirmed *p* type conductivity. The PEC characterization indicated an upper valence formed of copper orbital. The spectral dependence of the quantum efficiency has been analyzed to give the energy of the inter-band transitions.

Acknowledgments This work was supported partially by the Technical and Scientific Research Centre of Physico-Chemical Analysis (CRAPC). The authors would like to thank Dr R. Brahimi for comments concerning the structure refinement

References

1. Barnabé A, Mugnier E, Presmanes L, Tailhades Ph (2006) Mater Lett 60:3468
2. Aroutiounian VM, Arakelyan VM, Shahnazaryan (2005) Sol Energy 78: 581
3. Gurunathan K, Baeg JO, Lee SM, Subramanian E, Moon SGEJ, Kong KJ (2008) Catal Comm 9:395
4. Koumoto K, Koduka H, Seo WS (2001) J Mater Chem 11:251
5. Sun SS, Fan Z, Wang Y, Winston K, Bonner CE (2005) Mater Sci Eng B 116:279
6. Jovan V, Perne M, Petrovčič J (2010) Energ Convers Manag 51:2467
7. Bassaid S, Chaib M, Omeiri S, Bouguelia A, Trari M (2009) J Photochem Photobiol Chem 20:62
8. Bellal B, Saadi S, Koriche N, Bouguelia A, Trari M (2009) J Phys Chem Solids 70:1132
9. Ketir W, Bouguelia A, Trari M (2009) Desalination 244:144
10. Trari M, Töpfer J, Doumerc JP, Pouchard M, Ammar A, Hagenmuller P (1994) J Solid State Chem 111:104
11. Brahimi R, Bellal B, Bessekhouad Y, Bouguelia A, Trari M (2008) J Cryst Growth 310:4325
12. Mugnier E, Barnabé A, Tailhades P (2006) Solid State Ionics 177:607
13. Saadi S, Bouguelia A, Trari M (2006) Sol Energy 80:272
14. Trari M, Töpfer J, Dordor P, Grenier JC, Pouchard M, Doumerc JP (2005) J Solid State Chem 178:2751
15. Doumerc JP, Blangero M, Pollet M, Carlier D, Darriet J, Berthelot R, Delmas C, Decourt R (2009) J Electron Mater 38:1078
16. Nagarajan R, Duan N, Jayaraj MK, Li J, Vanaja KA, Yokochi A, Draeseke A, Tate J, Sleight AW (2001) Int J Inorg Mater 3:265
17. Muguerra H, Colin C, Anne M, Julien MH, Strobel P (2008) J Solid State Chem 181:2883